

Low-Frequency Unstable Planetary Waves in Realistic Basic States

BY

H.I. TANAKA

Contents

1. Introduction	61
2. Governing Equations	63
3. Results for Zonal Basic States	67
4. Results for Zonally Varying Basic State	75
5. Concluding Summary	79
Appendix	80
References	81

Abstract

This study investigates low-frequency, unstable planetary waves in realistic basic states of January 1979, using three-dimensional spectral primitive equations derived by orthonormal vertical structure functions and Hough harmonics. Eigenfrequencies, modal structures, and energetics are contrasted for different unstable modes. Three selected unstable modes are extensively examined. One is the Green mode in the planetary waves, and the other two are deep Charney modes having different meridional structures. We find that the Green mode of wavenumber 1 in the zonally varying basic state shows notable transient growth in the first internal vertical component during its life-cycle. One of the deep Charney modes becomes stationary at a preferred geographical location with nearly barotropic structure. The other deep Charney mode, which shows a monopole structure in the zonal basic state, becomes a dipole structure in the zonally varying basic state. The northern part of the dipole structure shows westward propagation with transient growth at a preferred location. The results suggest that large-scale Pacific blocking during the winter are, at least in part, related to the low-frequency Charney mode having a dipole structure. A possible connection between the amplification of planetary waves and the Green mode in zonally varying basic states is also discussed.

1. Introduction

The problem of large amplification of planetary waves attracts increasingly more attention in association with low-frequency variabilities in the atmosphere. Energetics analyses of the observed circulation field often assert an enhanced baroclinic conversion in the amplified planetary waves, implying that the amplification involves a process of baroclinic

instability (*e.g.*, Schilling, 1986). However, the linear stability analyses of planetary waves with zonal basic states (*e.g.*, Simmons and Hoskins, 1976; Hartmann, 1979) indicate major discrepancies with observation. The expected growth rate is insufficient to explain the amplification, the unstable planetary waves propagate eastward, and the wave structure of the most unstable mode is confined to the

troposphere, even though less unstable mode may penetrate into the deep atmosphere.

Comprehensive case studies of blocking episodes during the First GARP (Global Atmosphere Research Program) Global Experiment (FGGE) indicate that synoptic baroclinic waves feed large amount of energy into the planetary waves by means of an up-scale, nonlinear energy cascade (*see* Hansen and Chen, 1982; Kung and Baker, 1986; Holopainen and Fortelius, 1987). Long-term statistics of blocking formations also suggest an important role of high-frequency transient eddies in reinforcing the vorticity field of blocking waves (*see* Colucci, 1985; Mullen, 1987). Although energetics analyses and the enstrophy budget may be helpful in understanding the cause of blocking formations, the characteristic structure and behavior of blockings are not fully explained by the energy redistribution due to the wave-wave interaction.

Unstable eigenmodes in a zonally varying basic state were numerically investigated by Simmons *et al.* (1983), using a barotropic model. They demonstrated that various tropical forcings tend to excite a unique unstable normal mode in the model atmosphere. Moreover, with his two-layer, quasi-geostrophic model, Frederiksen (1982) showed that the zonal asymmetry of the basic state reorganizes the synoptic baroclinic waves to yield the Atlantic and Pacific storm tracks. Presumably his high-frequency synoptic disturbances are associated with Charney type instability in a zonal basic state. He also found blocking-like unstable modes with a dipole structure among a number of unstable solutions. He proposed that the dipole unstable mode explains the onset of the blocking formation. However, the physical explanation of the dipole modes seems less clear than the high-frequency synoptic disturbances. Although Frederiksen and Bell (1987) have extended his model to a five-layer tropospheric model, the

structure and behavior of their eigenmodes in planetary waves are too complicated to relate to the well-known unstable Charney and Green types in a zonal basic state. It is desirable to compare both the unstable modes in a zonal basic state and those in a zonally varying basic state. It is also desirable to use primitive equations because the quasi-geostrophic equations involve quasi-nondivergent and quasi-geostrophic assumptions, which may affect eigensolutions for planetary waves.

The objective of this study is to investigate the low-frequency, unstable planetary waves in realistic global basic states of January 1979 during the FGGE. This study supplements the work by Tanaka (1989) and Tanaka and Sun (1990). The eigenfrequencies, modal structures, and energetics of low-frequency unstable solutions are contrasted for zonal and zonally varying basic states in order to examine the effect of zonal asymmetry of the basic state on the low-frequency, unstable planetary waves. For that purpose, we have solved linearized, three-dimensional spectral primitive equations with a basis of three-dimensional normal mode functions (3-D NMFs) of motionless atmosphere. The use of the normal mode expansion is advantageous for stability analysis in that the matrix size for the eigenvalue problem can be effectively reduced by retaining only the rotational mode basis, and excluding the gravity mode basis. Thus, it is possible to analyze atmospheric eigenmodes with primitive equations, not only for zonal basic states but also for zonally varying basic states. Although our eigenvalue problem may be solved for any realistic basic state, complicating the basic state might cause the modal identification and physical interpretation of the eigensolutions to be lost. In this study, we consider a zonally varying basic state which is specified by a steady wavenumber 2, superimposed on the zonal mean basic state.

First, the governing equations in terms of the three-dimensional, spectral primitive

equations are reduced to the eigenvalue problem. The results for the zonal basic states are presented to identify the unstable modes with Charney (1947) and Green (1960) modes in previous research. We then examine how the zonal asymmetry of the basic state modulates the unstable planetary waves. Finally, we discuss the relation between the results of low-frequency unstable modes and the observed large-scale Pacific blocking and the amplification of wavenumber 1 during the winter season.

2. Governing Equations

2.1 Primitive Equations with a Static Stability Parameter

A system of primitive equations with a spherical coordinate of longitude λ , latitude θ , pressure p , and time t may be reduced to three prognostic equations of horizontal motions and thermodynamics for three dependent variables of (u, v, ϕ) . Here, u and v are the zonal and meridional components of the horizontal velocity V . The variable ϕ is a departure of the local isobaric geopotential from the reference state geopotential ϕ_0 , which is related through the hydrostatic equation to the reference state temperature T_0 . Using a matrix notation, these primitive equations (refer to Holton, 1975; Tanaka, 1985) may be written as

$$M \frac{\partial U}{\partial t} + LU = N + F, \tag{1}$$

where

$$U = (u, v, \phi)^T, \tag{2}$$

$$M = \text{diag} (1, 1, -\frac{\partial}{\partial p} \frac{p^2}{R\gamma} \frac{\partial}{\partial p}), \tag{3}$$

$$L = \begin{pmatrix} 0 & -2\Omega \sin\theta & \frac{1}{a \cos\theta} \frac{\partial}{\partial \lambda} \\ 2\Omega \sin\theta & 0 & \frac{1}{a} \frac{\partial}{\partial \theta} \\ \frac{1}{a \cos\theta} \frac{\partial}{\partial \lambda} & \frac{1}{a \cos\theta} \frac{\partial}{\partial \theta} & 0 \end{pmatrix}, \tag{4}$$

$$N = \begin{pmatrix} -V \cdot \nabla u - \omega \frac{\partial u}{\partial p} + \frac{\tan\theta}{a} uv \\ -V \cdot \nabla v - \omega \frac{\partial v}{\partial p} - \frac{\tan\theta}{a} vu \\ \frac{\partial}{\partial p} \left(\frac{p^2}{R\gamma} V \cdot \nabla \frac{\partial \phi}{\partial p} + \omega p \left(\frac{p}{R\gamma} \frac{\partial \phi}{\partial p} \right) \right) \end{pmatrix}, \tag{5}$$

$$F = \left(F_u, F_v, \frac{\partial}{\partial p} \left(\frac{pQ}{C_p \gamma} \right) \right)^T, \tag{6}$$

The left-hand side of (1) represents linear matrix operator M and L and a dependent variable vector U . The right-hand side represents a nonlinear term vector N and a diabatic term vector F , which includes the zonal F_u and meridional F_v components of frictional forces and a diabatic heating rate Q . The superscript T demotes a transpose, the symbol a represents the earth's radius, Ω the angular speed of the earth's rotation, R the specific gas constant, C_p the specific heat at a constant pressure, and ∇ the horizontal del-operator. Refer to Table 1 for symbols,

Table 1. Symbols, definitions, and variables

λ	longitude
θ	latitude
p	pressure
t	time
s	zonal wavenumber
l	meridional index
m	vertical index
S	truncation of s
l	truncation of l
M	truncation of m
T_0	reference state temperature
ϕ_0	reference state isobaric geopotential
u	zonal wind speed
v	meridional wind speed
ϕ	isobaric geopotential deviation from ϕ_0
V	horizontal wind velocity
z	height (vertical velocity = dz/dt)
ω	vertical p -velocity (= dp/dt)
γ	static stability parameter
a	radius of the earth
g	earth's gravity
Ω	angular speed of earth's rotation
R	specific gas constant of dry air
C_p	specific heat at constant pressure
F_u	zonal component of frictional force

Table 1-continued

F_i	meridional component of frictional force
Q	diabatic heating rate
p_0	surface pressure of reference state
t	dimensionless time scaled by 2Ω
∇	horizontal del-operator
δ_{ij}	Kronecker delta
i	imaginary unit
M	linear matrix operator given by (3)
L	linear matrix operator given by (4)
U	dependent variable vector $(u, v, \phi)^T$
N	nonlinear term vector given by (5)
F	diabatic term vector given by (6)
h_m	equivalent height
c_m	phase speed of gravity waves associated with h_m
X_m	scaling matrix for U
Y_m	scaling matrix for F
$\langle \cdot, \cdot \rangle$	inner product defined by (12)
$\text{diag}(\cdot)$	diagonal matrix
$(\cdot)^T$	transpose of a vector
$(\cdot)^*$	complex conjugate
$(\cdot)_R$	real part
$(\cdot)_I$	imaginary part
(\cdot)	time-independent basic state
$(\cdot)_{s,l,m}$	a component of indices s, l, m
$(\cdot)_i$	abbreviation of $(\cdot)_{s,l,m}$ used for perturbations
$(\cdot)_j$	abbreviation of $(\cdot)_{s,l,m}$ used for perturbations
$(\cdot)_k$	abbreviation of $(\cdot)_{s,l,m}$ used for basic states
$(\cdot)_s$	a component of a wavenumber s
$(\cdot)_{m=0}$	barotropic component
$(\cdot)_{m \neq 0}$	barotropic component
Π_{slm}	3-D NMF in a resting atmosphere
α_{slm}	dimensionless eigenfrequency of Laplace's tidal equation
w_{slm}	expansion coefficient of U
f_{slm}	expansion coefficient of F
r_{ijk}	real interaction coefficient for indices i, j, k
K	dimension of a system (14)
N	matrix size of a system (16)
w	dependent variable vector $(w_1, \dots, w_N)^T$
f	external forcing vector $(f_1, \dots, f_N)^T$
B	complex matrix associated with w
C	complex matrix associated with w^*
D	real diagonal matrix composed of α_i
b_{ij}	(i, j) entry of B given by (20)
c_{ij}	(i, j) entry of C given by (21)
ν	eigenfrequency of systems (24) and (26)
ξ, ζ	eigenvectors of systems (24) and (26)
E_i	perturbation energy of a component i (i.e., s, l, m)
$C(B, E)$	energy transformation from a basic state to perturbations
M_1	deep Charney mode (stationary mode)
M_2	deep Charney mode (dipole mode)
M_C	shallow Charney mode
M_i	internal Green mode

definitions, and variables used in this study. The vertical p-velocity ω is related to mass divergence, and the static stability parameter γ is given by

$$\gamma = \frac{RT_0}{C_p} - p \frac{dT_0}{dp}, \quad (7)$$

in which T_0 is assumed to be a function of p alone. In (5), as seen in Holton (1975), a vertical advection term of perturbation temperature is retained discarding the vertical change of γ in order to satisfy an energy conservation requirement.

2.2 Spectral Primitive Equation

In order to obtain spectral primitive equations, we assume that the vectors U and F in (1) can be approximated by a finite series of three-dimensional, normal mode functions in a resting atmosphere, $\Pi_{slm}(\lambda, \theta, p)$:

$$U(\lambda, \theta, p, t) = \sum_{s=-S}^S \sum_{l=-L}^L \sum_{m=-M}^M w_{slm}(t) X_m \Pi_{slm}(\lambda, \theta, p), \quad (8)$$

$$F(\lambda, \theta, p, t) = \sum_{s=-S}^S \sum_{l=-L}^L \sum_{m=-M}^M f_{slm}(t) Y_m \Pi_{slm}(\lambda, \theta, p), \quad (9)$$

Here the expansion coefficients $w_{slm}(t)$ and $f_{slm}(t)$ are the functions of time alone. The subscripts represent zonal wavenumbers s , meridional indices l , and vertical indices m . They are truncated at S , L , and M , respectively. The scaling matrices should be defined for each vertical index as:

$$X_m = \text{diag}(c_m, c_m, c_m^2), \quad (10)$$

$$Y_m = \text{diag}(2\Omega c_m, 2\Omega c_m, 2\Omega), \quad (11)$$

where c_m is a phase speed of gravity waves in shallow water, associated with the equivalent height h_m . The expansion basis $\Pi_{slm}(\lambda, \theta, p)$ is given by a tensor product of vertical structure functions (vertical normal modes) and Hough harmonics (horizontal normal modes). It is

known that they form a complete set and satisfy an orthonormality condition under an inner product $\langle \cdot, \cdot \rangle$ as:

$$\begin{aligned} \langle \Pi_{slm}, \Pi_{s'T'm'} \rangle &= \\ \frac{1}{2\pi p_s} \int_0^{p_s} \int_{-\pi/2}^{\pi/2} \int_0^{2\pi} \Pi_{slm}^* \cdot \Pi_{s'T'm'} \cos\theta d\lambda d\theta dp & \\ = \delta_{ss'} \delta_{ll'} \delta_{mm'} &, \end{aligned} \quad (12)$$

where the asterisk denotes the complex conjugate, the symbols δ_{ij} is the Kronecker delta, and the surface pressure p_s is treated as a constant near the earth's surface.

Applied to the inner product for (1), the weak form of primitive equation becomes

$$\langle M \frac{\partial U}{\partial t} + LU - N - F, Y_m^{-1} \Pi_{slm} \rangle = 0. \quad (13)$$

Substituting (8) and (9) into (13), rearranging the time-dependent variables, and evaluating the remaining terms, we obtain three-dimensional spectral primitive equations with external forcing terms,

$$\begin{aligned} \frac{dw_i}{dt} + i\sigma_i w_i &= -i \sum_{j=1}^K \sum_{k=1}^K r_{ijk} w_j w_k + f_i, \\ i &= 1, 2, \dots, K, \end{aligned} \quad (14)$$

where $t = 2\Omega t$, $K = (2S+1)(L+1)(M+1)$, i the imaginary unit, and σ the dimensionless eigenfrequencies obtained as a solution of Laplace's tidal equation with a basic state at rest. For simplicity, the three triple subscripts slm , $s'T'm'$, and $s''T''m''$ have been shortened to subscripts i , j , k , respectively. There should be no confusion in the use of i for a subscript even though it is used for the imaginary unit. The real interaction coefficients r_{ijk} are explicitly evaluated by the triple product of the basis functions. Analytical expression is available for derivatives of $\Pi_{slm}(\lambda, \theta, p)$. We should note here that the zonal wavenumbers s , s' , and s'' run from the negative integer $-S$ to the positive integer S , including zero, by definition of the Fourier series.

According to the Galerkin procedure above,

the system satisfies the same boundary conditions as 3-D NMFs in a resting atmosphere. Thus for the boundary conditions it may be reasonable to assume a vanishing kinematical wind, $(u, v, dz/dt) = 0$, near the lower surface and a bounded energy at the upper limit of the atmosphere (see Staniforth et al., 1985). The application of such a 3-D NMF expansion is widely seen in the nonlinear normal mode initialization technique which provides successful initial data for prediction models.

2.3 Perturbation Method

Next, if we introduce a perturbation method using notations \bar{w}_i and \bar{f}_i for time-independent basic states and w_i and f_i for small perturbations superimposed on the basic states (the same symbols with the original variables are used for convenience), the equation for the first-order term of perturbations becomes

$$\frac{dw_i}{dt} + i\sigma_i w_i = -i \sum_{j=1}^K \left(\sum_{k=1}^K (r_{ijk} + r_{kji}) \bar{w}_k \right) w_j + f_i, \quad (15)$$

$$i = 1, 2, \dots, K,$$

where the modal index k is used for the basic state and i and j for the perturbations. Since the negative zonal wavenumbers represent complex conjugates of the positive zonal wavenumbers, we can rewrite the equation above in terms of a matrix form for $s \geq 0$:

$$\frac{d}{dt} W + iDW = -iBW - iCW^* + F, \quad (16)$$

where

$$W = (w_1, \dots, w_i, \dots, w_N)^T, \quad \text{for } s \geq 0, \quad (17)$$

$$F = (f_1, \dots, f_i, \dots, f_N)^T, \quad \text{for } s \geq 0, \quad (18)$$

$$D = \text{diag}(\sigma_1, \dots, \sigma_i, \dots, \sigma_N), \quad (19)$$

and $N = (S+1)(L+1)(M+1)$. The (i, j) entries of the complex matrices B and C , namely b_{ij} and c_{ij} , are determined by the expansion coefficients of the basic state:

$$b_{ij} = \sum_{k=1}^K (r_{ijk} + r_{kij}) \bar{w}_k, \quad i, j=1, 2, \dots, N \text{ for } s' \geq 0, \quad (20)$$

$$c_{ij} = \sum_{k=1}^K (r_{ijk} + r_{kij}) w_k, \quad i, j=1, 2, \dots, N \text{ for } s' < 0, \quad (21)$$

In this study, an inviscid and adiabatic eddy will be examined, disregarding F for perturbations. Both B and C vanish for a basic state at rest ($\bar{w}_k = 0$), thus the equation (16) satisfies Laplace's classical tidal theory.

2.4 Eigenvalue Problem

For a zonal basic state ($\bar{w}_k \neq 0$ if $s''=0$), the matrix B becomes a real block diagonal ($b_{ij} \neq 0$ if $s = s'$), and C vanishes. Consequently, (16) can be solved for each (s, s') block:

$$\frac{d}{dt} W_s = -iD_s W_s - iB_s W_s, \quad s=1, 2, \dots, S, \quad (22)$$

where the subscripts represent wavenumbers of (s, s') blocks associated with perturbation vectors W_s . Because (22) is linear, we can assume the solution of W_s to be

$$W_s(t) = \xi \exp(-i\nu t). \quad (23)$$

The initial value problem (22) is then reduced to an eigenvalue problem for a real matrix with eigenvectors ξ and eigenvalues ν as:

$$\nu \xi = (D_s + B_s) \xi. \quad (24)$$

For a zonally varying basic state, both matrices B and C in (16) become complex, full matrices. Because of the complex conjugate term, we can not simply assume an exponential-type solution as in (23). In this case the complex matrices and variables are split into real and imaginary parts (given subscripts of R and I), and a solution is sought in the form:

$$\begin{pmatrix} W_R \\ W_I \end{pmatrix} (t) = \begin{pmatrix} \xi \\ \zeta \end{pmatrix} \exp(\nu t). \quad (25)$$

The eigenvalue problem for (16) then becomes:

$$\nu \begin{pmatrix} \xi \\ \zeta \end{pmatrix} = \begin{pmatrix} B_I + C_I & B_R - C_R + D \\ -B_R - C_R - D & B_I - C_I \end{pmatrix} \begin{pmatrix} \xi \\ \zeta \end{pmatrix}. \quad (26)$$

For complex eigenpairs the real-valued eigensolutions are given by

$$\begin{pmatrix} W_R \\ W_I \end{pmatrix} (t) = 2 \exp(\nu_R t) \begin{pmatrix} \xi_R \\ \zeta_R \end{pmatrix} \cos \nu_I t - \begin{pmatrix} \xi_I \\ \zeta_I \end{pmatrix} \sin \nu_I t. \quad (27)$$

Equations (24) and (26) are thus to be solved for zonal and zonally varying basic states in the subsequent sections.

2.5 Truncation

In this study, twelve vertical structure functions ($m = 0-11$) are constructed numerically after Kasahara (1984) with 24 Gaussian levels. The vertical index $m = 0$ is called an external (barotropic) modes, and $m = 1-11$ are called internal (baroclinic) modes which have m nodes in the vertical. The numerical internal modes are the discrete approximation of the continuous spectrum. Table 2 lists the reference state temperature T_0 on the 24 Gaussian levels and the obtained equivalent heights h_m for $m = 0-11$. The global mean temperature for the FGGE year (see Tanaka, 1985) is interpolated onto the Gaussian levels up to 30 mb, and the temperature of the standard atmosphere is substituted above this level. The temperature profile for the FGGE year is very close to that for every monthly mean. The difference is at

Table 2. The reference state temperature T_0 at the 24 Gaussian levels and the equivalent heights h_m for the vertical modes $m = 0-11$.

Level	T_0 (K)	Level	T_0 (K)	m	h_m (m)
1	253.78	13	262.63	0	9746.5
2	226.08	14	267.89	1	3457.7
3	215.39	15	272.26	2	777.5
4	211.41	16	275.92	3	269.3
5	206.01	17	279.03	4	113.9
6	208.23	18	281.71	5	46.9
7	216.04	19	284.04	6	24.1
8	223.23	20	286.03	7	13.5
9	231.44	21	287.66	8	7.7
10	240.42	22	288.94	9	3.7
11	248.86	23	289.83	10	1.2
12	256.31	24	290.33	11	0.1

most 2K at the lower troposphere. Since the higher order internal modes have a problem of aliasing in the stratosphere and above (refer to Sasaki and Chang, 1985; Staniforth *et al.*, 1985), only the first seven vertical structure functions ($m = 0-6$) are applied to the subsequent computations (*i.e.*, $M=6$). Figure 1 illustrates these vertical structure functions. They may be suitable for the representation of planetary waves because they provide adequate vertical resolutions throughout the troposphere and the stratosphere. As is demonstrated by the resolution test in the Appendix, the unstable modes in the planetary waves have almost converged by this vertical resolution.

The Hough vector functions are computed using semi-normalized associated Legendre polynomials with 120 Gaussian latitudes so that the integral is exact up to the triple product of the basis functions. The meridional indices l contain two distinct modes: gravity-inertial modes and rotational modes of the Rossby-Haurwitz type. One advantage of Hough mode expansion is an efficient reduction of the matrix size of the instability problem by retaining the rotational modes alone, excluding the gravity mode basis. As is shown in the Appendix, excluding the gravity mode basis

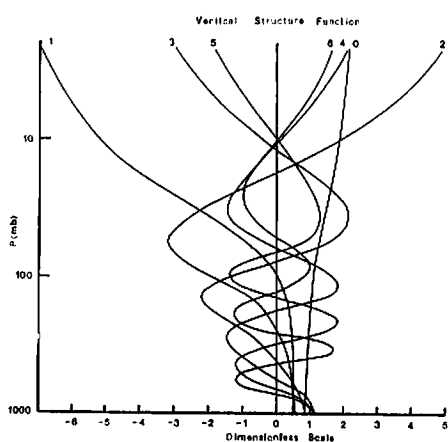


Fig.1 Vertical structure functions for vertical indices $m = 0-6$. Values of corresponding equivalent heights are seen in Table 2.

does not affect the unstable solution of planetary waves. Moreover, the unstable solutions have almost converged with meridional truncation $L = 18$ using the rotational modes. We choose $L = 18$ in this study. In addition, we include the Kelvin mode using a numbering of $l = -1$ because the observed energy level is exceptionally large among the gravity modes. According to the observed energy spectra by Tanaka (1985), these vertical and meridional truncation represent about 90% of the total energy of the atmosphere.

3. Results for Zonal Basic States

3.1 Basic State

Unstable eigenmodes are examined for two different zonal basic states: a zonal wind profile of a 30° jet described by Simmons and Hoskins (1976) and the observed monthly-mean field of January 1979. The 30° jet profile has a separable structure in the vertical and the meridional, and is deliberately chosen to be barotropically stable (refer to Simmons and Hoskins, 1976). The January basic state is compiled with the FGGE III-b data assimilated by the Geophysical Fluid Dynamics Laboratory. Figure 2 illustrates the latitude-height section of the observed monthly-mean zonal wind field reproduced by $m''=0-6$ and $l''=0-18$ of the geostrophic modes.

3.2 Growth Rates and Phase Speeds

The growth rates and phase speeds of the first-three unstable modes are plotted in Fig. 3 as functions of the zonal wavenumbers $s=1-10$. This is a result of antisymmetric solutions with the 30° jet basic state. Since the stratosphere is not considered in Simmons and Hoskins' 30° jet, we first compute the fastest growing modes using a constant $\gamma = 30$ K (cross mark), and compare them with Simmons and Hoskins' results (white circles). The value of the constant γ represents its vertical average (*see* Table 1 of Tanaka, 1985). The agreement is

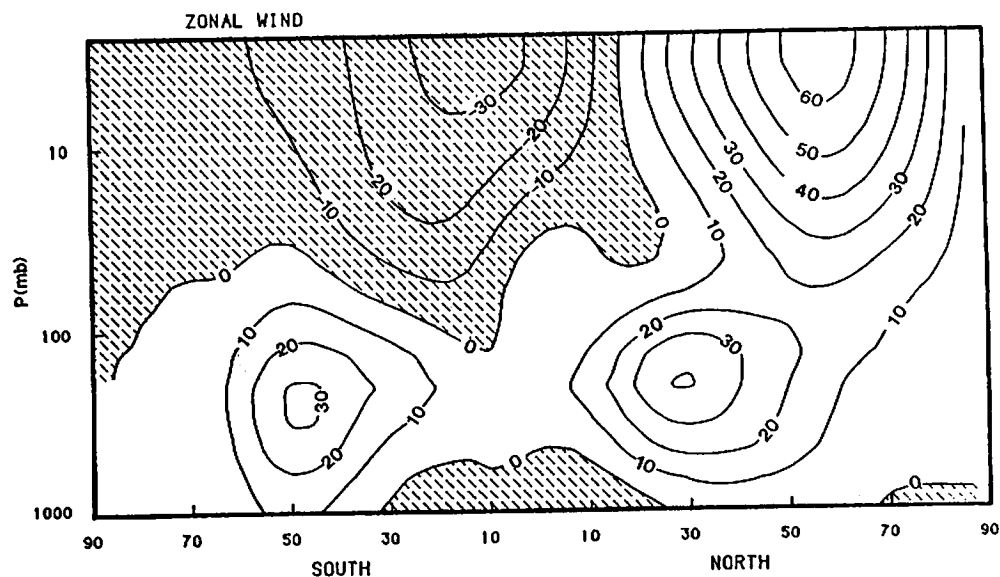


Fig.2 The latitude-height section of the observed zonal wind (m/s) for a monthly mean of January 1979, reproduced by $l''=1.18$ and $m''=0.6$.

within a reasonable range. Henceforth the results are based on the temperature profile in Table 2. A pronounced Charney-type baroclinic instability (labeled M_c) appears with the e-folding time of about 2.0 (day) at $s=7-8$ with the phase speed of about 9° /day). Contrasted with the result by Simmons and Hoskins (1976), we find that the stable layer in the stratosphere reduces the growth rate for $s > 6$, and the maximum growth rates shift toward smaller wavenumbers. According to Ioannou and Lindzen's (1986) analytical solutions, the unstable modes in the figure, M_c , M_2 , and M_1 can be identified as Charney modes with different meridional structures. The phase speed of M_1 is very slow in the planetary waves, whereas that of M_2 is fast (about 9° /day). The distinct phase speeds of these unstable modes were also detected by Gall (1976) and Zhang and Sasamori (1985).

Figure 4 illustrates the same curves but for the January basic state. For the basic state having a global extension, the unstable modes are partitioned in the northern and southern hemispheric modes according to the analysis of

their structure. The results in Fig. 4 are of the northern hemispheric modes, and a similar result has been obtained by a symmetric extension of the northern basic state toward the Southern Hemisphere. Contrasted with Fig. 3 we find the growth rate of M_c decreases in the planetary waves, and the maximum growth rates of M_1 and M_2 shift toward the planetary wave range. As a result, M_1 and M_2 become the dominant unstable modes at $s=1-2$, and $s=3-4$. Further experiments show that the up-scale shift of M_1 and M_2 are caused mainly by the small meridional scale of the basic state in the mid- to lower-troposphere resulting from the tropical and polar easterlies. The results are consistent with those documented by Zhang and Sasamori (1985). The shallow Charney mode M_c seems to have changed to the Green mode M_G in the planetary waves (Green, 1960).

3.3 Structures

The latitude-height structures of the geopotential field for M_1 , M_2 , M_G , and M_c for the January basic state are illustrated in Fig. 5.

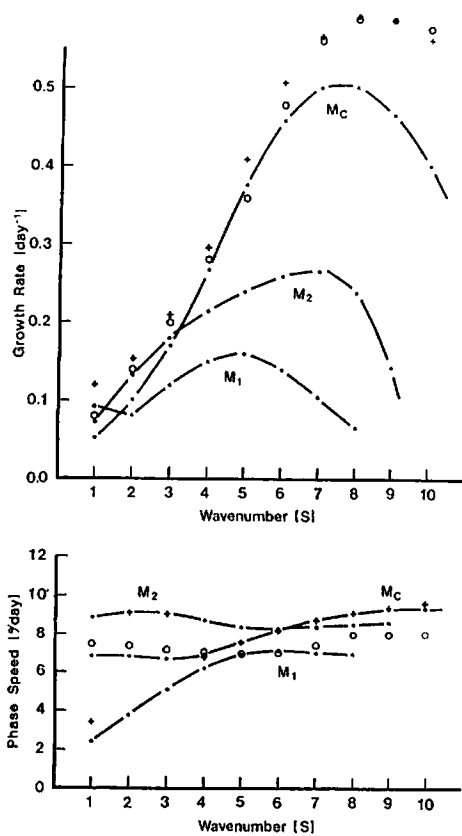


Fig.3 Growth rates and phase speeds of the first three unstable modes (labeled M_c , M_2 , and M_1) as functions of wavenumbers $s=1-10$ for a zonal basic state of Simmons and Hoskins' 30° jet. The cross marks denote the fastest growing modes for constant static stability profile, $\gamma=30$ K, and white circles denote the results of Simmons and Hoskins (1976).

The structure of M_c at $s=6$ shows an amplitude maximum at the upper troposphere in mid-latitudes, indicating a westward phase tilt with height. These results resemble those obtained by Hartmann (1979) in which a typical winter basic state is used. The structure of wavenumber 8 shows an amplitude maximum near the surface in mid-latitude, indicating a westward phase tilt with height. The tilt implies a northward heat transport, which would release zonal available potential energy. The structure, and thus the eddy heat and momentum transports, is consistent with

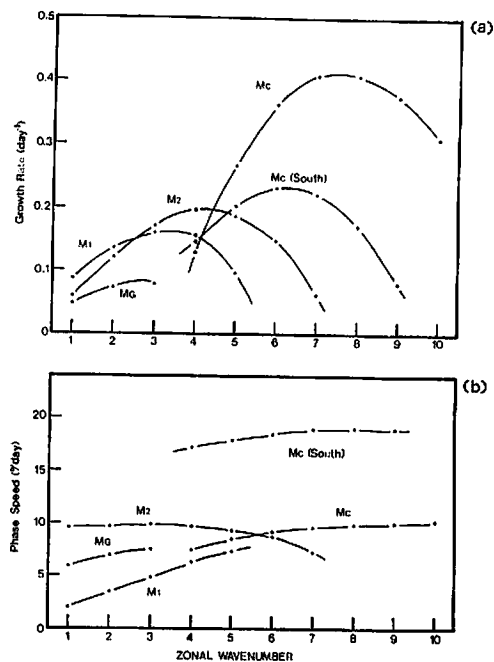


Fig.4 As in Fig. 3 but for a zonal basic state of January 1979. M_c is the shallow Charney mode, and M_1 , M_2 , the deep Charney modes. M_G is regarded as Green mode. M_c (south) is that appearing in Southern Hemisphere.

Simmons and Hoskins' results. We are convinced that the method of 3-D NMF expansion is useful for studying baroclinic instability. At planetary waves, the growth rates in Fig. 4 are competing, and the solution is hardly obtainable with the time integration method as discussed by Simmons and Hoskins. That, however, is not the case for the present eigenvalue problem. The structure of M_2 shows a westward phase tilt with height, but indicates a characteristic northwest-southeast phase tilt in the horizontal plane. This phase structure distinguishes M_2 from M_c . The monopole structure of amplitude becomes dipole in the higher zonal waves as seen in Simmons and Hoskins' result. For the structure of M_2 at $s=3$, the amplitude maximum shifts northward near 60° N above the tropopause level, indicating a northwest-southeast phase tilt. The phase structure indicates a westward phase tilt

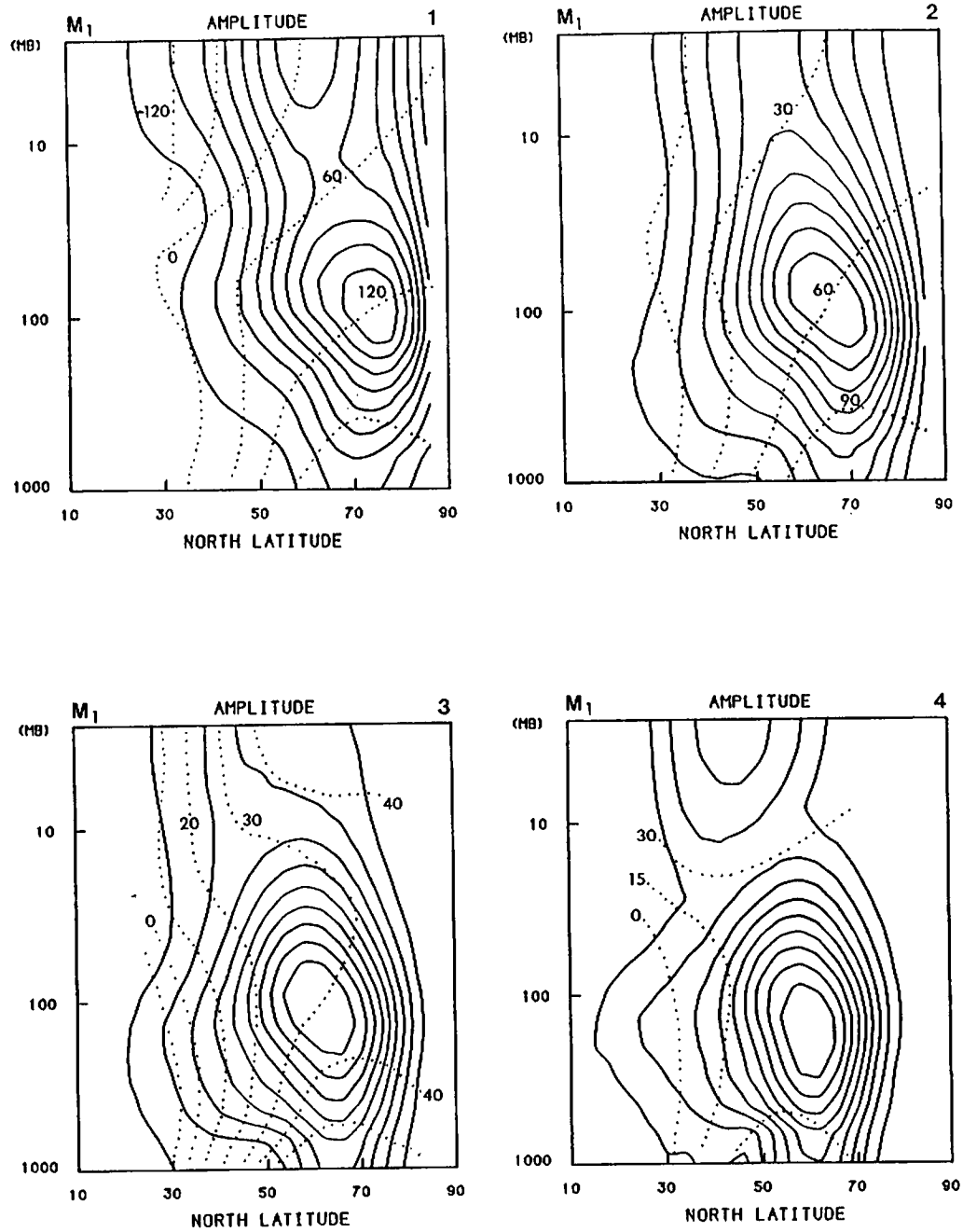
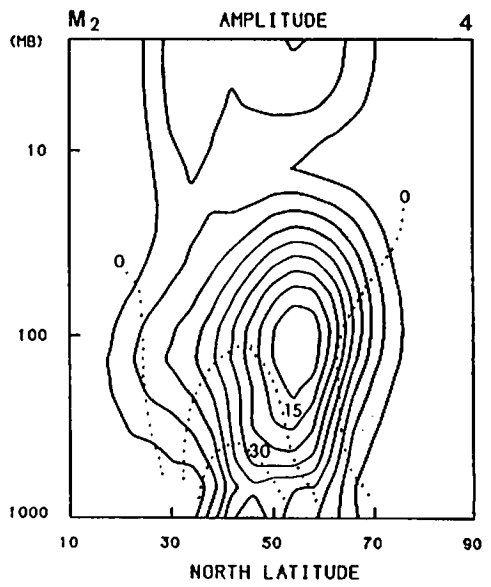
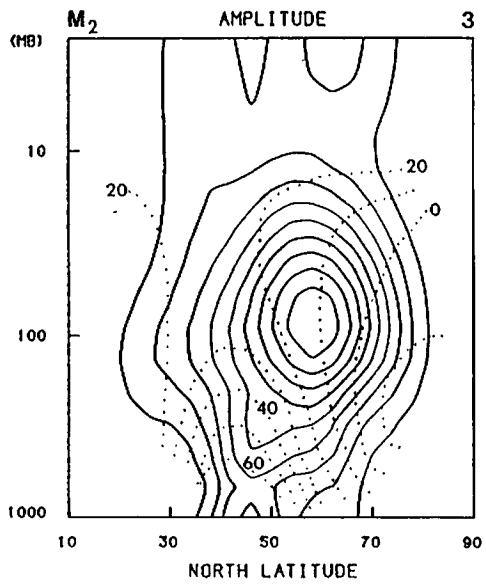
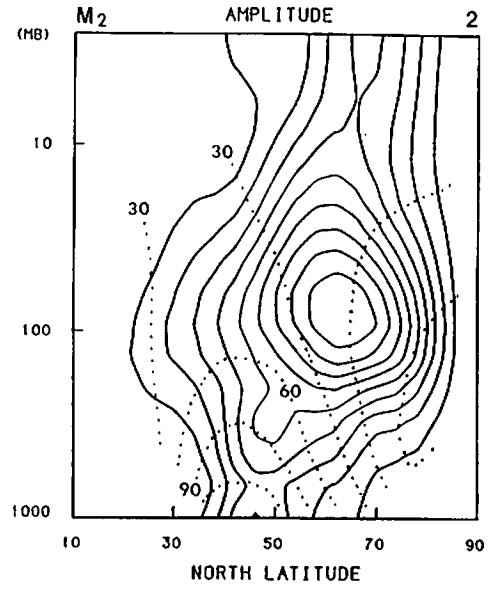
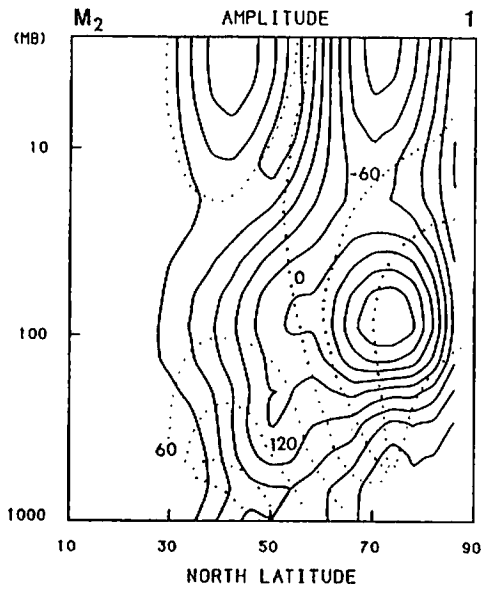
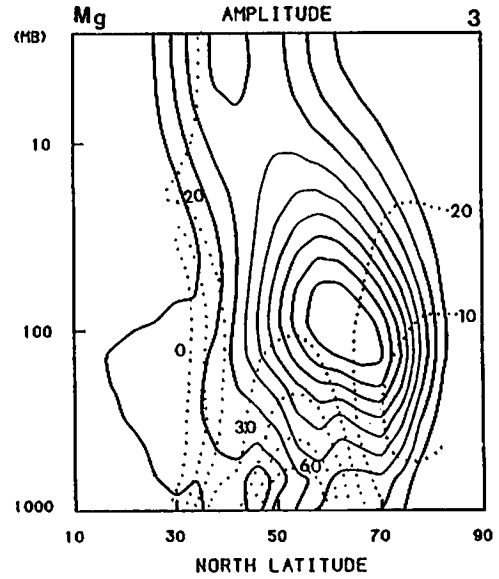
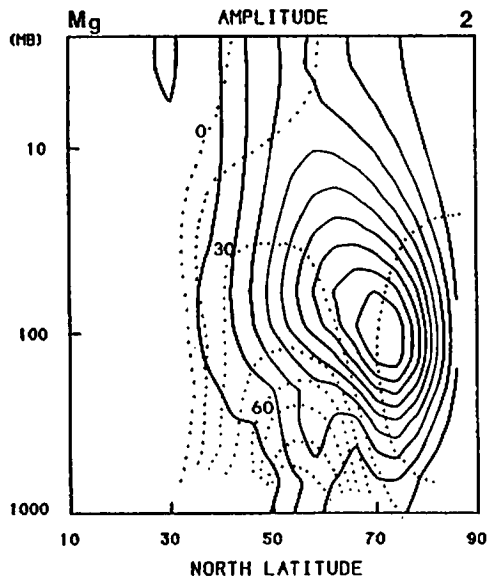
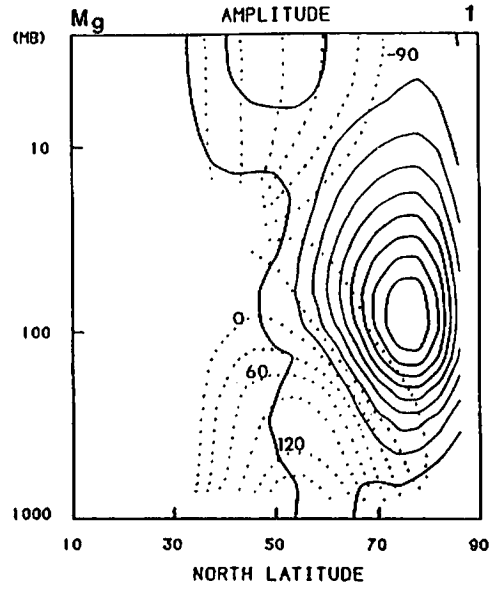
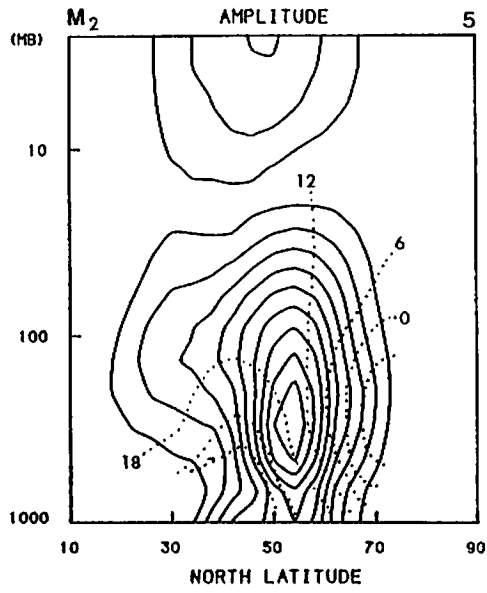
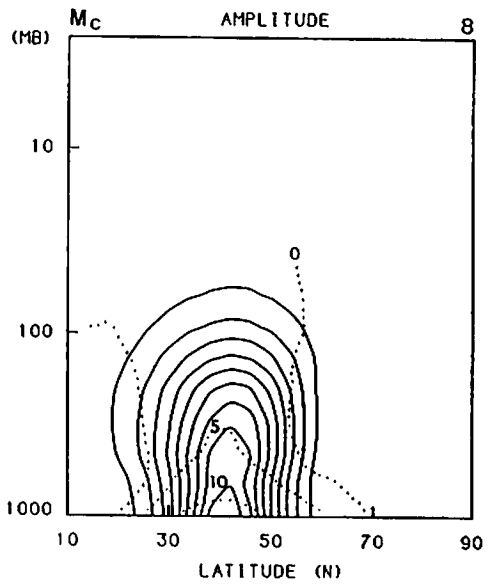
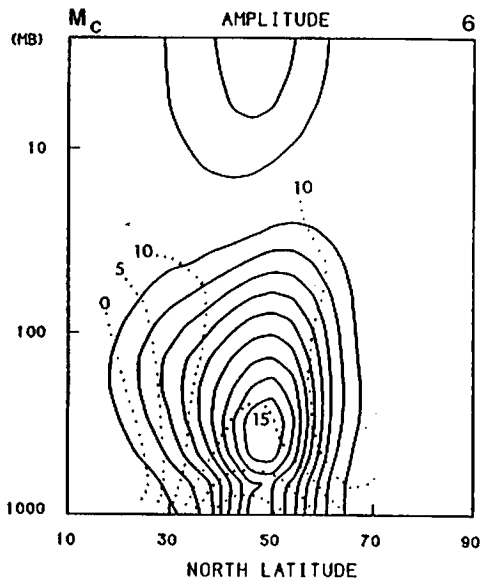
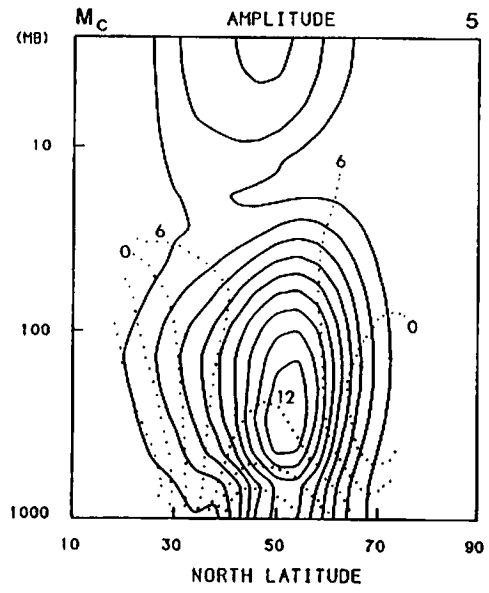
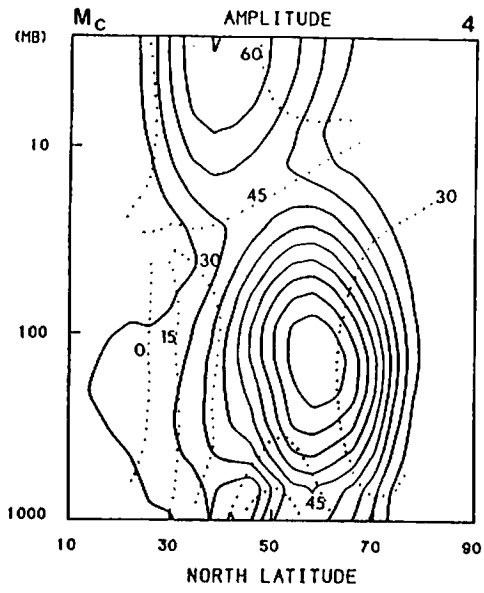


Fig.5 Latitude-height structures of geopotential amplitudes (solid line in arbitrary unit) and phases (dashed line denoting longitudes of ridges) of unstable modes (denoted at upper left) for each zonal wavenumber (upper right). Refer to Fig. 4 for the unstable mode names.







with height at mid-latitude, but the structure is nearly barotropic and out of phase at high latitudes. The structure of M_1 at $s=1$ shows an amplitude maximum at 100 mb in high latitudes and another peak in the upper stratosphere, indicating a monotonic westward phase tilt with height. This structure also closely resembles the results obtained by Hartmann (1979) and Zhang and Sasamori (1985), even though the former identifies M_1 as the deep Charney mode whereas the latter identifies it as the Green modes. In this study, M_1 and M_2 are identified as deep Charney modes by the results shown in Fig. 3 and 4. In addition, M_1 will be characterized by its large external component of $m=0$, which is typical of external Charney modes, contrasted with the dominant internal component of $m=1$ for Green mode. The location of high latitudes is necessary for deep Charney modes as Hartmann suggests.

3.4 Energetics

According to Kasahara and Puri (1981) and Tanaka (1985), an energy E_i for a particular basis function is defined in dimensional form by

$$E_i = \frac{1}{2} p_s h_m |w_i|^2. \quad (28)$$

The summation of E_i for all indices i represents a total of kinetic energy and available potential energy integrated over the mass of the atmosphere with an additional boundary term which is, in general, negligible. After a proper normalization of W_i , the energy levels for the most unstable modes of M_1 at $s=1$ and M_c at $s=6$ for the January basic state are plotted as functions of the vertical (Fig. 6) and meridional (Fig. 7) indices. The vertical energy spectra reveal bimodal distributions with peaks at $m=0$ and $m=2-4$. Energy levels drop significantly at $m=5, 6$, and contributions from the truncated higher-vertical indices are expected to be small. On the other hand, the

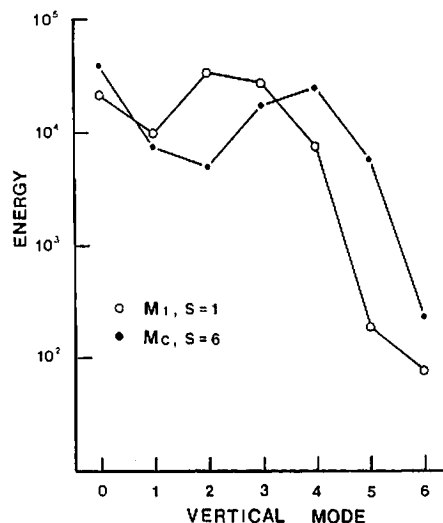


Fig.6 Normalized energy spectra for M_1 at $s=1$ and M_c at $s=6$ in the vertical index domain, resulting from the summation of all meridional indices.

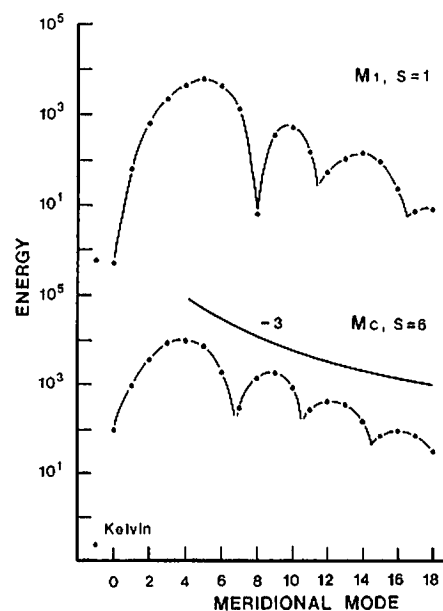


Fig.7 As in Fig. 6 but for the energy spectra in the meridional index domain for the barotropic components.

largest portion of barotropic energy resides in the meridional indices $l = 3-6$, with some energy gaps in the higher indices. The fact that the energy levels are quite smaller for both Kelvin modal indices and the higher indices confirms that the meridional truncation was reasonable. It is interesting to note that these energy spectra of the unstable eigensolutions coincide with the spectra observed by Kasahara and Puri (1981) and Tanaka (1985).

Because of the meridional wind shear, not only the baroclinic instability but also the barotropic instability is expected to account for the energy supply of unstable normal modes. In order to explore the origin of this energy supply, an energy flow box diagram describing energy interactions between barotropic and baroclinic components is constructed. By differentiating (28) with respect to time and substituting (22), we obtain

$$\begin{aligned} \frac{dE_i}{dt} &= 2\Omega p_s h_m \Sigma_j \text{Re}(ib_{ij}^* w_j^* w_i)_{m''=0} \\ &\quad + 2\Omega p_s h_m \Sigma_j \text{Re}(ib_{ij}^* w_j^* w_i)_{m'' \neq 0} \\ &= C(B_{m''=0}, E_i) + C(B_{m'' \neq 0}, E_i) \end{aligned} \quad (29)$$

The first term of the right-hand side of (29) stands for energy transformations from the barotropic component of the zonal field $B_{m''=0}$ into E_i , and the second term represents those from the baroclinic components of the zonal field $B_{m'' \neq 0}$ into E_i . By adding all indices for $m=0$, and for $m \neq 0$, (29) becomes:

$$\frac{dE_{m=0}}{dt} = C(B_{m''=0}, E_{m=0}) + C(B_{m'' \neq 0}, E_{m=0}), \quad (30)$$

$$\frac{dE_{m \neq 0}}{dt} = C(B_{m''=0}, E_{m \neq 0}) + C(B_{m'' \neq 0}, E_{m \neq 0}). \quad (31)$$

The resulting energy flow box-diagrams are presented in Fig. 8 for the most unstable modes of M_1 at $s=1$ and M_c at $s=6$. Upper boxes ($m'' \neq 0, m \neq 0$) denote the baroclinic component and lower boxes ($m''=0, m=0$) the barotropic components. Energy transformations are normalized to yield the percentile contributions to the growth.

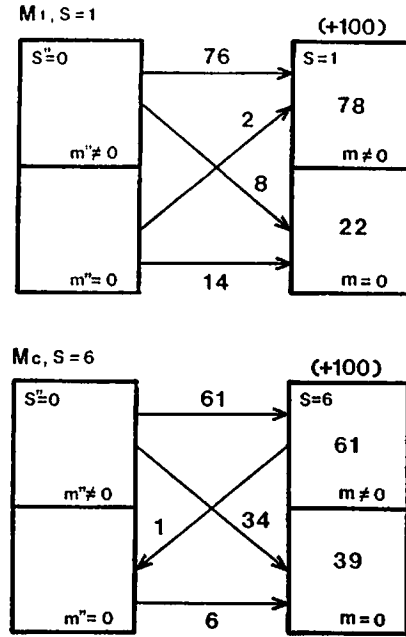


Fig. 8 Energy flow box diagram for M_1 at $s=1$ and M_c at $s=6$. Upper boxes ($m'' \neq 0, m \neq 0$) denote the baroclinic components and lower boxes ($m'' = 0, m = 0$) the barotropic components. Energy transformations are normalized to yield the percentile contributions of the growth. Percentile energy is read in the boxes.

Percentile energy is read in the boxes. It is shown that large proportions of energy are transformed from zonal baroclinic energy to eddy baroclinic energy for the growing modes. These energy flows essentially result from baroclinic instability, whose major energy source is the available potential energy. The energy supply from $m'' \neq 0$ amounts to 84% of the total supply for M_1 at $s=1$ and 95% of the supply for M_c at $s=6$. Similar energy characteristics are obtained for the unstable mode M_2 at $s=3$.

4. Results for a Zonally Varying Basic State

4.1 Basic State

We will consider a zonally varying basic state which is specified by a steady wavenumber 2 superimposed on the zonal-mean basic state.

Figure 9 illustrates the latitude-height section of geopotential height of the wavenumber 2 for January 1979, reproduced by the composition of $m''=0-6$ and $l''=0-18$. We will call this a wave 2 basic state, and distinguish it from the zonal basic state in Fig. 2. It has a global extension, although the figure is illustrated for only the Northern Hemisphere. The amplitude of the wave 2 basic state in the Southern Hemisphere is small. Since a basic state chosen in this manner involves only even zonal waves ($s''=0$ and 2), the eigenspace of (26) becomes a direct sum of eigenspace for even zonal waves ($s=0,2,4,\dots$) and odd zonal waves ($s=1,3,5,\dots$).

4.2 Low-Frequency Unstable Modes

In this study, we will concentrate on selected low-frequency unstable modes in the planetary waves. The eigenvalue problem of (26) is solved with a zonal truncation of $S=2$ in order to identify the low-frequency unstable modes. With this truncation, (16) for the odd waves

becoms

$$\frac{d}{dt} W_1 = -iD_1 W_1 - iB_1 W_1 - iC_1 W_1^*. \quad (32)$$

Note that (32) is identical to (22) for $s=1$ except for an additional complex conjugate term arising from the wave 2 basic state. We may thus isolate the effect of the wave 2 basic state on the unstable modes of wavenumber 1. The first term on the right-hand side of (32) indicates phase speeds of neutral modes under a motionless atmosphere. The second term describes zonal-wave interactions. The unstable modes gain their energy through down-scale energy transformations from the zonal field. In contrast, the last complex conjugate term can be recognized as wave-wave interactions, and the growing modes gain their energy through the up-scale energy transformations from the steady zonal asymmetry. Table 3 lists the growth rates and periods of the three fastest-growing modes in the Northern Hemisphere. The results for the zonal basic state are also

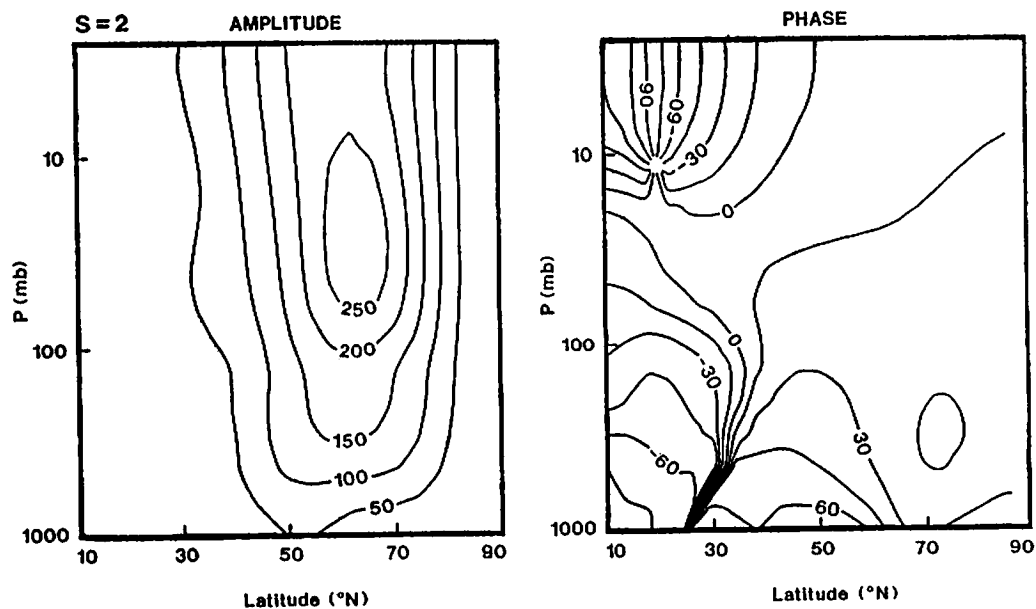


Fig.9 The latitude-height section of the observed geopotential height of the wavenumber 2 for January 1979 used as a basic state. Amplitude (m) and phase (longitude of ridge) are reproduced by $l''=0-18$ and $m''=0-6$.

Table 3. Mode names, growth rates, and eigenperiods of the three fastest-growing modes of $s=1$ in the zonal basic state (left) and in the nonzonal basic state (right) for the case of zonal truncation $S=2$.

Zonal basic state			Nonzonal basic state		
mode	growth rate (1/day)	period (day)	mode	growth rate (1/day)	period (day)
1 M_1	0.087	181	1 M_1	0.156	∞
2 M_2	0.047	61	2 M_2	0.078	33
3 M_3	0.059	37	3 M_3	0.069	35

listed (see Fig. 4). We can identify these low-frequency unstable modes as M_1 , M_2 , and M_G of $s=1$. It is worth noting that the slow-moving mode M_1 becomes stationary.

Figure 10 displays the elliptic oscillations of the first-three dominant components of M_2 and M_G depicted for the oscillatory factor of $w_{slm}(t)$ in (27). Integers in the parentheses denote (s, l, m) , and dots on the trajectories describe the initial phase of the time evolutions. In the zonal basic state these trajectories depict pure circles indicating an eastward propagation. For M_2 , two barotropic components show retrogression indicating clear principal axes, while the baroclinic component shows progression. This means that some of the Hough mode projections show westward propagation for its barotropic component with a period of about 35 days. For M_G , the first internal component ($m=1$) grows significantly during its life-cycle with 53-day period. The trajectory is regarded almost as a standing oscillation with periodic amplification in the stratosphere.

4.3 Structures

In conjunction with the component-wise elliptic oscillations of Eq. (27), the total energy of a mode, defined by the summation of E_i in (28), oscillates with a half period of the life-cycle. We may define a mature stage of the modal life-cycle by one of the two energy

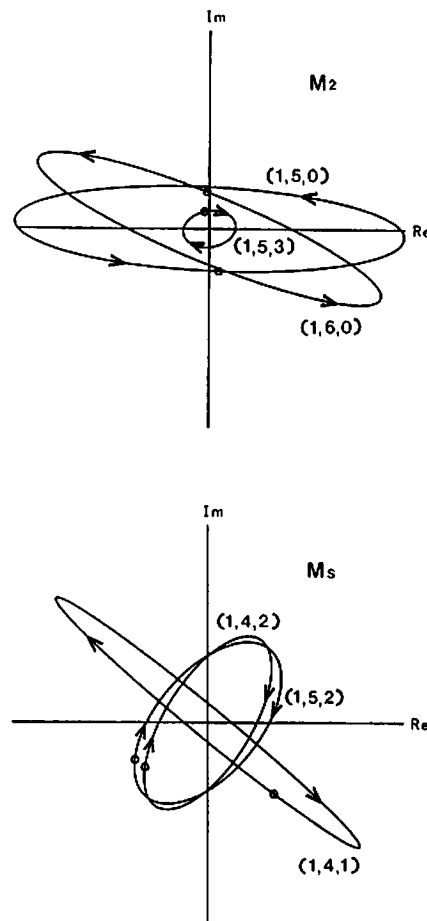


Fig.10 Trajectories of elliptic oscillations of w_{slm} (see Eq. 27) on a complex plane for dominant components of M_2 and M_G at $s=1$. Integers in the parentheses denote (s, l, m) , and dots on the trajectories indicate the arbitrary initial phases of the time evolution. The values are multiplied by gh_m to have a unit of geopotential.

peaks. Such a definition is not required for the stationary unstable mode except for the alternative sign of the eigenvector. Figure 11 illustrates the meridional-height structures of the geopotential field for M_1 , M_2 , and M_G in the Northern Hemisphere at their mature states. These are the solutions of $s=1$ in (32) obtained for a global basic state. For the stationary mode M_1 the influence of the wave 2 basic state is clear in the phase change, being

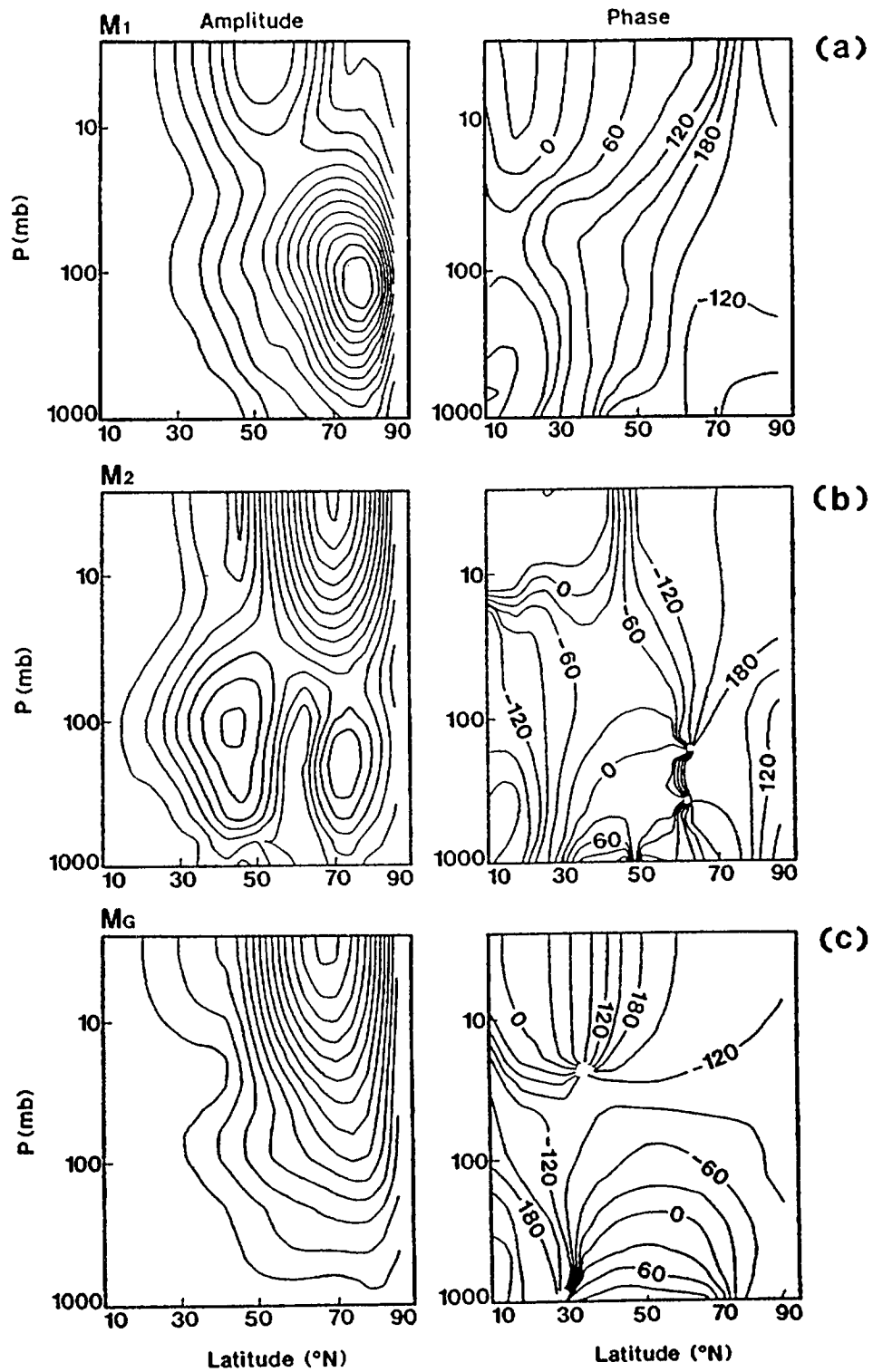


Fig.11 Latitude-height structures of geopotential amplitudes and phases for (a) M_1 , (b) M_2 , and (c) M_G of wavenumber 1 at the mature stages of their life-cycles.

of equivalent barotropic structure. A pronounced amplitude maximum appears at 75° N, 100 mb level with the ridge around 120° W. Similar stationary modes appear also in Frederiksen (1982) and Simmons *et al.* (1983). Mode M_2 exhibits two amplitude maxima at 75° N and 45° N at the tropopause level with opposite phases. The northern pole produces a ridge around 180° W with barotropic structure. Moreover, the northern ridge of the solution propagates westward. Contrasted with the monopole structure in the zonal basic state (Fig. 6), we find that the zonal asymmetry of the basic state changes the Charney mode M_2 to be a dipole structure. Mode M_C produces the amplitude maximum at 65° N in the upper stratosphere with broader meridional extent. The phase tilts westward with altitude. The dominant contribution from $m=1$ of M_C is a typical characteristic of the Green mode even though its nodal structure is not clear by the complicated basic state.

5. Concluding Summary

This study investigates low-frequency, unstable planetary waves in realistic global basic states of January 1979 and Simmons and Hoskins' 30° jet, using three-dimensional spectral primitive equations derived by orthonormal vertical structure functions and Hough harmonics. The eigenfrequencies, modal structures, and energetics of the low-frequency, unstable solutions have been presented.

At least four distinct unstable modes are identified:

1. Shallow Charney mode M_1 has its e-folding time of about 2 days, and the maximum growth rate is seen at the synoptic-scale zonal wavenumbers ($s=7-8$). This mode is shallow in its structure in a sense that it is trapped within the troposphere and will not penetrate into the deep atmosphere.
2. Dipole-Charney mode M_2 has one node

in the meridional structure compared with the shallow Charney mode which has no node. This mode dominates at the zonal wavenumbers $s=3-4$.

3. Monopole-Charney mode M_1 has largest meridional and vertical structure. The vertical structure indicates that the largest energy is contained at the external component, which is the common characteristics of Charney modes.
4. Green mode M_C indicates the largest amplitude within the middle atmosphere. The vertical energy spectrum indicates its energy peak at the first internal component.

Contrasting the results for zonal and zonally varying basic states, we have shown that the zonal asymmetry of the basic state changes the basic features of the low-frequency unstable modes. Their major changes are examined with the properties of wavenumber 1. The Green mode of wavenumber 1 in the zonally varying basic state shows notable transient growth during its life-cycle (53-day) in the first internal vertical component. One of the deep Charney modes M_1 turns out to be stationary at a preferred geographical location with a nearly barotropic structure. Frederiksen (1982) and Simmons *et al.* (1983) have analyzed similar stationary modes. The other deep Charney modes M_2 , which shows a monopole structure in the zonal basic state, becomes a dipole structure during its life-cycle (35-day) in the zonally varying basic state. It is found in this study that the blocking-like dipole modes in Frederiksen and Bell (1987) are identified as dipole Charney modes modulated by the zonal asymmetry of the basic state.

The results of the present study suggest that not only the fastest growing modes but also the second and third fastest unstable modes are important for many atmospheric events. The shallow Charney mode is important in exciting synoptic disturbances as the major energy source for atmospheric eddies. The dipole

Chaney mode may be related to the formation of blocking anticyclone; the monopole Charney mode to the steady planetary waves; and the Green mode to the stratospheric sudden warming. Further study is expected to compare the unstable modes in the planetary waves with observed weather phenomena.

Acknowledgments

The author is grateful to Dr. E. C. Kung, Professor of the University of Missouri-Columbia for his guidance and financial support during my stay in Missouri and to Dr. A. Kasahara of the National Center for Atmospheric Research for his meaningful discussion on this study.

Appendix

The vertical and meridional resolution tests

Vertical normal modes for the primitive equations with the basic state at rest are identical to those for the quasi-geostrophic potential vorticity equation on mid-latitude β -plane. For this reason, the latter equation is used for the vertical resolution test. The linearized equation for meridionally independent perturbations may be written as

$$\frac{f_0^2}{R\gamma}(\sigma^2\phi)'' - n^2\phi + \frac{1}{U-c}(\beta - \frac{f_0^2}{R\gamma}(\sigma^2U))\phi = 0, \quad (33)$$

where $\sigma = p/p_s$, $n = s/a \cos(45^\circ)$, and the primes denote vertical differentiations. Except for the use of $\gamma (= 30 \text{ K})$ defined in (7), all symbols have their conventional meanings.

The effect of vertical resolutions is then examined for the traditional Charney-Green problem with linear profile of U over $0 < \sigma < 1$ ($U = 30 \text{ m/s}$ at the top). The procedure to solve (33) is similar to that described in Section 2. Namely, assuming that the atmospheric variables belong to the subspace spanned by the series of vertical structure functions, and taking a natural inner product to obtain a system of ordinary differential equations, we then solve the algebraic matrix eigenvalue

problem for the stability analysis. The results of growth rates and phase speeds for wavenumbers $s=2, 6$, and 10 are illustrated in Fig. A1 as functions of vertical resolution M . As is described in Section 2, we prepare $2M$ vertical structure functions which are computed numerically after Kasahara (1984) using 120 Gaussian vertical levels. Then the first $M+1$ vertical structure functions ($m=0-M$) are used to solve $M+1$ by $M+1$ matrix eigenvalue problems. According to the results, wavenumber 2 seems to have converged with $M=6$ (at least for the growth rate), although wavenumber 10 requires even more vertical resolutions. The results demonstrate that the vertical normal mode expansion is applicable to the instability problem, particularly to the planetary waves.

The effect of meridional truncations and the exclusion of gravity mode basis are examined

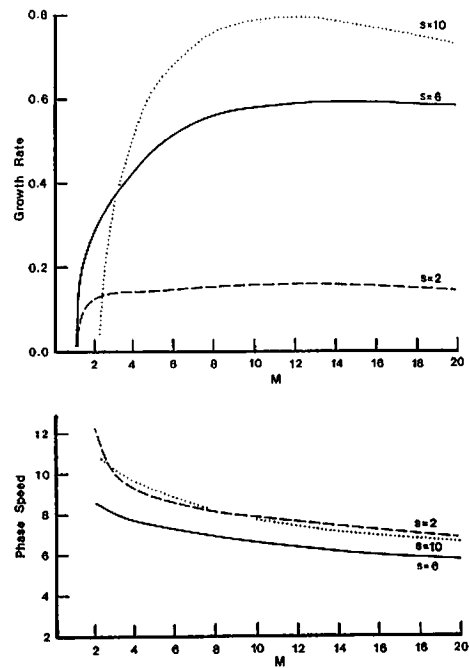


Fig. A1 Growth rates (day^{-1}) and phase speeds c_R (ms^{-1}) of the most unstable modes at wavenumbers $s=2, 6$, and 10 as functions of vertical resolutions M .

for the basic state of Simmons and Hoskins' 30° jet using the spectral primitive equations as described in Sections 2 and 3. The vertical advection of perturbation temperature in (5) is neglected here by a scaling analysis. The results of growth rates and phase speeds for the most unstable modes at $s=2, 6,$ and 10 are illustrated in Fig. A2 as functions of meridional truncation L . The results of $L=48$ represent the use of Rossby mode basis $l=0-24$, added with 12 eastward gravity modes and 12 westward gravity modes basis. Evidently, the solutions have converged with the truncation of $L=18$, and the gravity mode basis shows insignificant effect on the unstable solutions.

For ageostrophic zonal basic states, such as the January basic state in this study, we obtain high-frequency unstable gravity modes which appear independently of the Charney-Green type instability. Although such unstable gravity modes must be important for the geostrophic

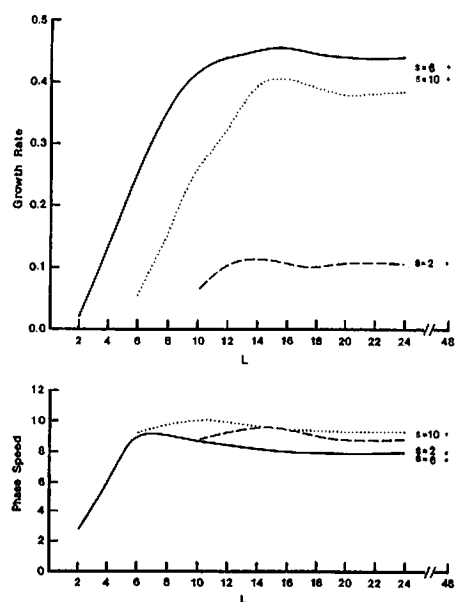


Fig. A2 Growth rates (day^{-1}) and phase speeds ($^{\circ} \text{day}^{-1}$) of the most unstable modes at wavenumbers $s=2, 6,$ and 10 as functions of meridional truncations L . The dots at $L=48$ represent the results including 24 gravity mode basis added with the Rossby mode basis of $l=0-24$.

adjustment, we have confirmed that the gravity mode basis is unimportant as long as Charney-Green type instability is concerned.

References

- Charney, J. G. (1947): The dynamics of long waves in a baroclinic westerly current. *J. Meteor.*, **4**, 135-162.
- Colucci, S. J. (1985): Explosive cyclogenesis and large-scale circulation change: Implications for atmospheric blocking. *J. Atmos. Sci.*, **42**, 2701-2717.
- Frederiksen, J. S. (1982): A unified three-dimensional instability theory of the onset of blocking and cyclogenesis. *J. Atmos. Sci.*, **39**, 969-982.
- Frederiksen, J. S. and Bell, R. C. (1987): Teleconnection patterns and the roles of baroclinic, barotropic and topographic instability. *J. Atmos. Sci.*, **44**, 2200-2218.
- Green, J. S. A. (1960): A problem in baroclinic instability. *Quart. J. Roy. Meteor. Soc.*, **86**, 237-251.
- Hansen, A. R. and Chen, T.-C. (1982): A spectral energetics analysis of atmospheric blocking. *Mon. Wea. Rev.*, **110**, 1146-1165.
- Hartmann, D. L. (1979): Baroclinic instability of realistic zonal-mean states to planetary waves. *J. Atmos. Sci.*, **36**, 2336-2349.
- Holopainen, E. and Fortelius, C. (1987): High-frequency transient eddies and blocking. *J. Atmos. Sci.*, **44**, 1632-1645.
- Holton, J. R. (1975): *The dynamic meteorology of the stratosphere and mesosphere*. Meteor. Monogr., **37**, Amer. Meteor. Soc., 218 pp.
- Ioannou, P. and Lindzen, R. S. (1986): Baroclinic instability in the presence of barotropic jets. *J. Atmos. Sci.*, **43**, 2999-3014.
- Kawahara, A. (1984): The linear response of a stratified global atmosphere to tropical thermal forcing. *J. Atmos. Sci.*, **41**, 2217-2237.
- Kawahara, A. and Puri, K. (1981): Spectral representation of three-dimensional global data by expansion in normal mode functions. *Mon. Wea. Rev.*, **109**, 37-51.
- Kung, E. C. and W. Baker, E. (1986): Spectral energetics of the observed and simulated northern hemisphere general circulation during blocking episodes. *J. Atmos. Sci.*, **43**, 2729-2812.
- Mullen, S. L. (1987): Transient eddy forcing of blocking flows. *J. Atmos. Sci.*, **44**, 3-22.
- Sasaki, Y. K. and Chang, L. P. (1985): Numerical solution of the vertical structure equation in the normal mode method. *Mon. Wea. Rev.*, **113**, 782-793.
- Schilling, H.-D. (1986): On atmospheric blocking

- types and blocking numbers. *Anomalous atmospheric flows and blocking*. Advances in Geophysics. **29**, Academic Press, 71-99.
- Simmons, A. J. and Hoskins, B. J. (1976): Baroclinic instability on the sphere: Normal modes of the primitive and quasi-geostrophic equations. *J. Atmos. Sci.*, **33**, 1454-1477.
- Simmons, A. J., Wallace, J. M. and Branstator, G. W. (1983): Barotropic wave propagation and instability and atmospheric teleconnection patterns. *J. Atmos. Sci.*, **40**, 1363-1392.
- Staniforth, A., Beland, M. and Côté, J. (1985): An analysis of the vertical structure equation in sigma coordinates. *Atmos.-Ocean*, **23**, 232-358.
- Tanaka, H. L. (1985): Global energetics analysis by expansion into three-dimensional normal mode functions during FGGE winter. *J. Meteor. Soc. Japan*, **63**, 180-200.
- Tanaka, H. L. (1989): A study of low-frequency unstable planetary waves in realistic zonal and zonally varying basic states. *Tellus.*, **41A**, 179-199.
- Tanaka, H. L. and Sun, S. (1990): A study of baroclinic energy sources for large-scale atmospheric normal modes. *J. Atmos. Sci.*, **47**, 2674-2695.
- Zhang, K.-S. and Sasamori, T. (1985): A linear stability analysis of the stratospheric and mesospheric zonal mean state in winter and summer. *J. Atmos. Sci.*, **42**, 2728-2750.